JOURNAL OF MATERIALS SCIENCE 32 (1997) 1365–1370

Catalytic effects of Ag_2O additives on microstructure and recrystallization in borate glasses

S. RAM*
Institute of Metal Research, Technical University of Berlin, Hardenbergstraße-36, D-10623, Berlin, Germany

K. RAM
Infrared Laboratory, DMSRDE Kanpur, Kanpur 208013, India

A substitution of Ag_2O for B_2O_3 in a $35BaO–25Fe_2O_3–(40-x)B_2O_3–xAg_2O$, $x = 0.0$, 0.5, 1.0 and 3.0, glass series modifies the B_2O_3 network and changes infrared frequencies in the 1600–600 cm^{-1} region. Four bands at 1440, 1280, 1180 and 1120 cm^{-1} appear in glass containing no Ag_2O additive. On adding the Ag_2O, the 1120 cm^{-1} band (which belongs to the $BO_3 \rightarrow BO_4$ modified group in the B_2O_3 network) no longer appears, and the other three bands (belonging to the B–O stretching vibrations in the interconnected boroxol rings) shift 15–40 cm^{-1} to higher frequencies expected in the reduced structural defects of $BO_3 \rightarrow BO_4$ modified groups and non-bridging oxygens. This modified glass crystallizes (at 500–850 °C) into acicular $BaFe_{12}O_{19}$ microcrystals of a higher coercivity of $\sim$5000 Oe, suitable for high energy-density magnets and other devices.

1. Introduction

The structure of pure and substituted borate glasses has been a topic of discussion over the last several years [1–5]. Infrared or Raman spectroscopy unambiguously confirms the fact that the vitreous v-B_2O_3 forms a network structure of planar six membered boroxol rings of BO_3 triangles. The v-B_2O_3 spectra (Raman) contain four distinct B–O stretching vibration frequencies at 1475, 1325, 1260 and 1210 cm^{-1} at room temperature [4]. X-ray diffractometry and other similar structural techniques do not directly take into account these short-range structures and do not apply here.

These studies were devoted to understanding and modelling the v-B_2O_3 glass structure and its changes on heating the specimen through the glass-transition temperature, T_g, or on partially substituting the B_2O_3 by alkali or other oxides. A knowledge of these parameters is important to design glasses and glass-ceramic products with particular physical properties. The configuration of the structural units of the glass, which, of course, changes on heating the specimen, determines the nucleation and growth (and governs the morphology of the crystallites) which maintains the equilibrium between crystallites and the glass matrix. For example, thin platelets of 1–2 mm thickness of $35BaO–25Fe_2O_3–40B_2O_3$ glass, if annealed between 500 and 850 °C, crystallize acicular-shaped $BaFe_{12}O_{19}$ microcrystals [6, 7], with an aspect ratio $\leqslant 20$. These acicular particles are geometrically convenient to cut down further (by milling) their size in single domain particles of ~ 1 μm.

A small, 0.5–3.0 mol%, addition of Ag_2O as a nucleation catalyst to this particular glass has been shown to improve crystallization yield of $BaFe_{12}O_{19}$ by a factor of ~ 2 on annealing between 575 and 795 °C [6]. In an attempt to understand the crystallization phenomena, we report infrared spectra of these glasses and those in which $BaFe_{12}O_{19}$ microcrystals crystallized. The results are discussed in the light of the magnetic properties of $BaFe_{12}O_{19}$ microcrystals.

2. Experimental procedure

The glasses of $35BaO–25Fe_2O_3–(40-x)B_2O_3–xAg_2O$ compositions (mol%), with $x = 0.0$, 0.5, 1.0 and 3.0, were prepared from the mixtures of anhydrous $BaCO_3$, α-Fe_2O_3, B_2O_3 and Ag_2O. In each case, a 10–20 g batch of the mixture was put into a platinum crucible, covered with a lid, and melted between 1200 and 1300 °C (by intermediate stirring of the melt with a thin quartz rod) for 15 min in an electric furnace. The liquid was then poured on to a copper plate (of sufficient volume and size to act as a heat sink) and quickly pressed by another similar plate to form 1–2 mm thick platelets. Several batches were prepared

* *Present address*: National Metallurgical Laboratory, Jamshedpur 831007, India.

0022–2461

TABLE I Structural and magnetic properties of virgin and recrystallized $BaO–Fe_2O_3–B_2O_3$ glasses with finely divided $BaFe_{12}O_{19}$ microcrystals.

Sample	Crystallization yield (wt%)	Magnetic properties		
		M_s(e.m.u. g^{-1})	H_{ci}(Oe)	T_C(°C)
$35BaO–25Fe_2O_3–40B_2O_3$ glass				
1. Virgin glass	–	0.1	50	–
2. Sample 1 annealed				
(i) 760 °C/2 h + 795 °C/25 h	18	13	2500	462
(ii) 575 °C/2 h + 795 °C/25 h	21	15	3100	457
(iii) 575 °C/5 h + 795 °C/58 h	21	15	3000	–
3. Sample (iii) milled, washed and annealed 3 h at 1000 °C[a]	–	71	4500	–
$35BaO–25Fe_2O_3–39B_2O_3–1Ag_2O$ glass				
4. Virgin glass	–	0.05	20	–
5. Sample 4 annealed 575 °C/5 h + 795 °C/58 h	37	27	1800	439
6. Sample 5 milled, washed and annealed 3 h at 1000 °C[a]	–	71	5000	435

[a] The magnetic $BaFe_{12}O_{19}$ particles were separated by milling the specimen to ~1 μm particle size under acetone followed by washing in hydrofluoric acid. The recovered powder was finally annealed at 1000 °C to have the improved magnetic properties.

in order to confirm that the sample is reproducible. All of the samples so prepared were found to be reasonably amorphous as analysed by X-ray diffractometry. These amorphous samples were recrystallized by thermal annealing at elevated temperatures as summarized in Table I.

Infrared spectra (300–4000 cm^{-1}) of the various amorphous and recrystallized specimens were measured as pellets in a KBr matrix using a Perkin–Elmer 783 IR spectrophotometer. The reported frequencies of the sharp bands of $BaFe_{12}O_{19}$ or B_2O_3 network are accurate to ± 2 cm^{-1} but the broad bands of the B_2O_3 network in the 1000–1800 cm^{-1} region have an accuracy of ± 10 cm^{-1} in ascertaining the peak positions. These accuracy values were determined by average values of the errors in measuring the data under selected experimental conditions.

The saturation magnetization, M_s, and intrinsic coercivity, H_{ci}, were measured on a vibrating sample magnetometer (aerosonic limited model VSM-3001). The Curie temperature, T_c, was determined from the thermomagnetogram, which was measured by heating the specimen (with a heating rate of 10 °C min^{-1}) between 25 and 600 °C, at a magnetic field of 1–2 kOe, using a similar magnetometer in conjunction with a high-temperature oven assembly to control and vary the temperature, as reported earlier [6, 7].

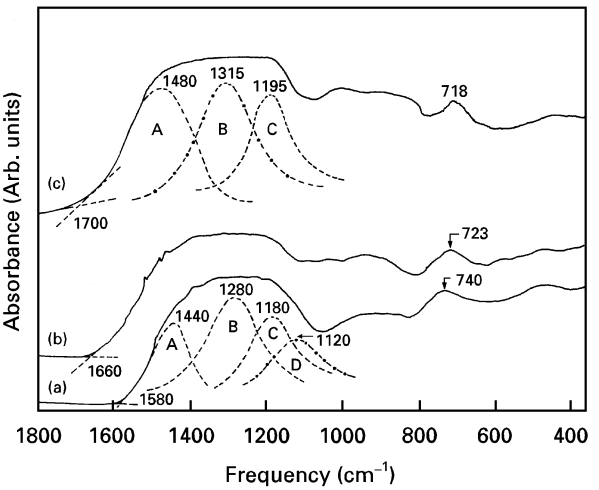

Figure 1 Infrared absorption spectra of $35BaO–25Fe_2O_3–(40-x)B_2O_3–xAg_2O$ glasses, (a) $x = 0$, (b) $x = 0.5$ and (c) $x = 3.0$. The dashed curves A, B, C and D represent approximate positions and shapes of the overlapping bands in the resultant experimental curves.

3. Results

3.1. Infrared spectra of virgin glasses

Fig. 1 summarizes the infrared spectra of virgin $35BaO–25Fe_2O_3–(40-x)B_2O_3–xAg_2O$ glasses, with (a) $x = 0$, (b) $x = 0.5$, and (c) $x = 3.0$. Spectrum (a), which is measured on the pure glass using no additive, has a broad absorption between 1580 and 1050 cm^{-1}, which apparently comprises four different bands (indicated by the dashed A, B, C and D curves). These bands overlap one another but could be identified by the variation of the intensity in the spectra recorded at a two to five times magnified scale of absorption and/or the frequency between 1000 and 1800 cm^{-1}. Also, in the magnified spectrum, the involved bands are not resolved separately, but the signatures of all four bands are better reproduced. For example, the bands A, B and C are clearly shown up at ~1480, 1315 and 1195 cm^{-1} in a typical spectrum shown in Fig. 2 for the glass with $x \sim 3$.

The half-bandwidth, ~450 cm^{-1}, in the total absorption between 1580 and 1050 cm^{-1}, is large, but the intensity rather sharply decreases on either side, demonstrating the presence of at least three overlapping bands in it. The fourth band, i.e. band D, is clearly shown by a small, but distinct, asymmetry in the drop of the intensity in the total absorption in the higher frequency side. A deconvolution of the measured infrared profiles (assuming the Gaussian shape of

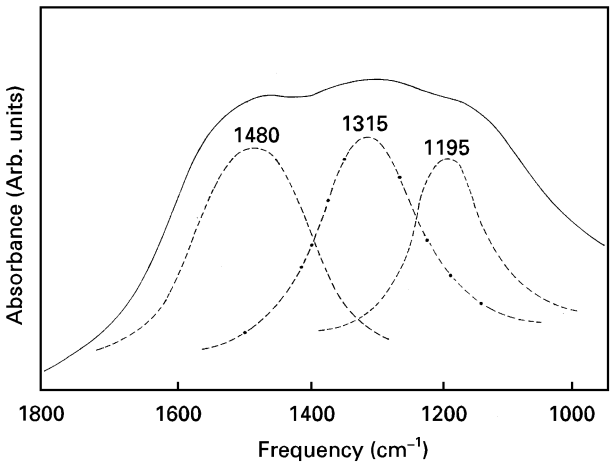

Figure 2 Infrared spectrum of the glass in Fig. 1c recorded at an expanded scale of the *y*-axis. The background is subtracted to show the realistic spectrum of the sample. The dashed curves are the same as in Fig. 1c.

the bands) using a standard fit and plot program (for the curve fitting) with help of a computer provided the positions and shapes of these bands, as shown by the dashed curves A, B, C and D in Fig. 1. The total area in the analysed bands fits the area under the observed spectrum within a difference of 20%. A better fit of the results is not feasible, in this example, in a large and monotonically increasing background absorption over the range 1800–400 cm^{-1}.

On adding Ag_2O in glasses (b) and (c), the band D either disappears or shifts to lower frequencies, causing less of a dip in the involved region. Moreover, the broad absorption extends ~120 cm^{-1} to higher frequencies, shown by the onset of zero absorption (defined by the intersection of two straight lines in the involved spectrum in Fig. 1) of the highest frequency band shifted from 1580 cm^{-1} in spectrum (a) to 1660 cm^{-1} in spectrum (b), and 1700 cm^{-1} in spectrum (c) in Fig. 1. Thus the bands A, B and C are positioned at 1480, 1315 and 1195 cm^{-1} in the Ag_2O catalysed glass (c). These bands have 15–40 cm^{-1} higher values than those in glass (a) using no Ag_2O additive, and compare well, within a difference of 5–15 cm^{-1}, with three characteristic B–O stretching vibrations observed in pure *v*-B_2O_3 at 1475, 1325 and 1210 cm^{-1} in the Raman spectrum [4].

It is noticed that the relative intensity of the infrared background absorption, especially in the 1050–400 cm^{-1} region, is two to three times enhanced in the BaO–Fe_2O_3–B_2O_3 ternary glasses than that reported in pure *v*-B_2O_3 or other typical binary or ternary borate glasses [8–13]. The enhanced background absorption does not allow resolution of the characteristically weak bands expected in the B–O bending vibrations and Fe–O stretching vibrations in the associated species in the glass. The total intensity and the relative intensity distribution in these bands are not influenced by the addition of Ag_2O in these glasses, but it clearly leads to a regular decrease in position of the band group at 800–600 cm^{-1}. For example, this band group appears at 740 cm^{-1} in glass (a), having no Ag_2O additive, and that is shifted at 723 cm^{-1} in glass (b) and at 718 cm^{-1} in glass (c) after 0.5 and 3 mol% Ag_2O additions, respectively.

3.2. Thermal treatments and crystallization of the glasses in separated magnetic $BaFe_{12}O_{19}$ particles

When annealed between 500 and 850 °C, these glasses crystallize $BaFe_{12}O_{19}$ microcrystals, which were identified by X-ray powder diffractometry. These microcrystals are homogeneously dispersed in the glass matrix, as is evident from the optical micrograph [6, 7], and have relatively sharp infrared bands between 640 and 320 cm^{-1} (Figs 3 and 4). The $BaFe_{12}O_{19}$ characteristic bands have been easily identified by comparison with the infrared spectrum of pure $BaFe_{12}O_{19}$ ceramic powder measured under the same conditions [11]. The positions (marked over the associated bands in Figs 3 and 4) of the bands marginally vary depending on (i) the $BaFe_{12}O_{19}$ particle size, (ii) the $BaFe_{12}O_{19}$ volume fraction, and (iii) the fraction(s) of the secondary crystalline phase(s), if any.

The Ag_2O catalysed glasses crystallize into separated magnetic particles of $BaFe_{12}O_{19}$ between 500 and 850 °C (cf. Table I). These crystallites were recovered by washing away the glassy part in hydrofluoric acid (which dissolves the glass and allows recovery of the crystallites). They result in a maximum ~37 wt% (~21 wt% otherwise) crystallization yield of the total specimen (against a theoretically expected

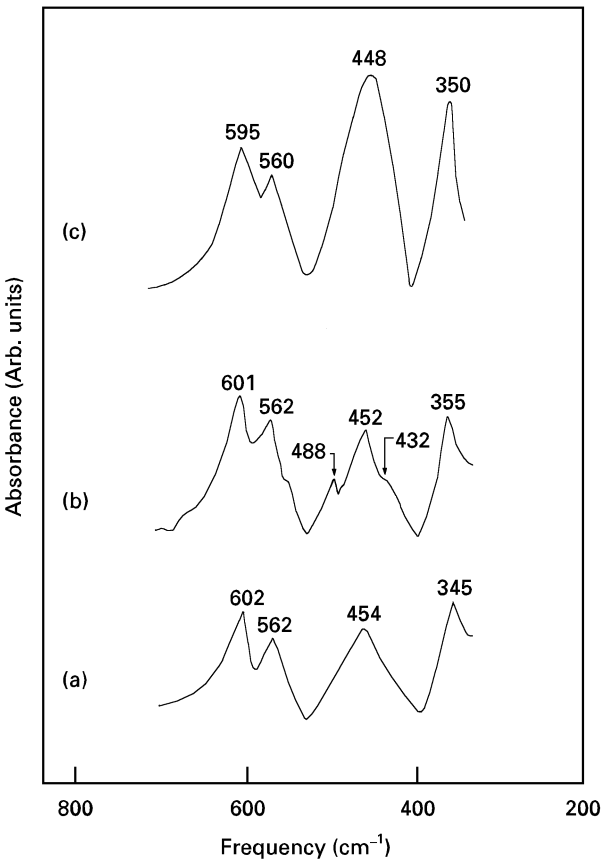

Figure 3 Infrared spectra of recrystallized glasses in the present series at 760 °C for 2 h followed by 2 h at 795 °C: (a) $x = 0.5$, (b) $x = 1.0$ and (c) $x \sim 3.0$.

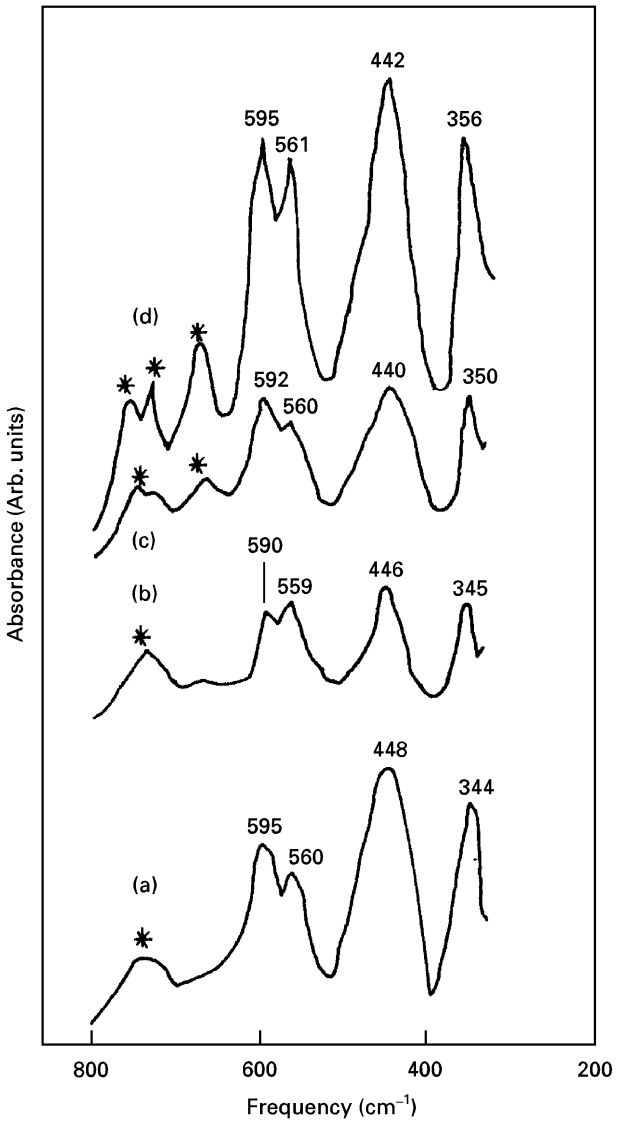

Figure 4 Infrared spectra of recrystallized glasses. (a) 35BaO–25Fe_2O_3–40B_2O_3 annealed 2 h at 760 °C and 25 h at 795 °C. (b) and (c) contain 1 mol% Ag_2O additive. These were annealed at 795 °C for (b) 2 h and (c) 25 h after 2 h at a common temperature of 575 °C. The intensities of the characteristic peaks (the positions are written over the peaks) of recrystallized $BaFe_{12}O_{19}$ particles are considerably enhanced on prolonged annealing of 5 h at 575 °C and 58 h at 795 °C in (d). (*) Peaks due to v-B_2O_3 or barium borates.

value of 37.6 wt% if all iron oxide in the glass is utilized to form $BaFe_{12}O_{19}$) in the glass having 1 mol% Ag_2O additive and crystallized 5 h at 575 °C and 58 h at 795 °C. This total specimen, along with the $BaFe_{12}O_{19}$ magnetic particles, measures a total saturation magnetization of $M_s = 27$ e.m.u. g^{-1} and an intrinsic coercivity of $H_{ci} = 1800$ Oe, as measured on a vibrating sample magnetometer (using a magnetic field to 20 kOe), at room temperature. The glass, using no Ag_2O, crystallized under these optimized conditions had a total $M_s = 15$ e.m.u. g^{-1}, but a considerably larger $H_{ci} = 3000$ Oe value, probably due to a peculiar microstructure developed with considerably larger volume fractions of non-magnetic particles of barium borates precipitated in the $BaFe_{12}O_{19}$ grain boundaries.

These grains are much bigger than the single domain size 0.2–1.0 μm for M-type (such as $BaFe_{12}O_{19}$) hexagonal ferrites [14, 15]. They were therefore cut, crushed and finally milled to ~1 μm size using an attrition-type machine. The powder obtained was carefully washed in hydrofluoric acid and a purely magnetic $BaFe_{12}O_{19}$ powder was recovered. At this stage, the specimen had several structural imperfections (introduced by the milling) and did not exhibit a high H_{ci} value. These imperfections are removed on thermal annealing (3 h) of the specimen at 1000 °C (insufficient to cause unwanted grain growth [15]), leading to an increase in H_{ci} from 1800 Oe to 5000 Oe, with $M_s = 71$ e.m.u. g^{-1}, at room temperature. The present H_{ci} value is ~1.5 times larger than that usually measured for A-grade M-type ferrites [15]. Similar refined $BaFe_{12}O_{19}$ powders, obtained without the Ag_2O addition in the primary glass, have the same M_s value, but $H_{ci} = 4500$ Oe.

4. Discussion

4.1. IR bands in the B_2O_3 network

In the pure v-B_2O_3, the boroxol rings are bridged together through the so-called "bridging oxygens" and result in a locally ordered network configuration, as discussed by several authors [1, 16, 17]. This ideal structure is modified in binary or ternary borate glasses, as in the present example, where part of the B_2O_3 is replaced by Fe_2O_3 and other oxides, which alone usually do not form a glass. In this case, these non-glass-forming oxides are irregularly bridged (or trapped) in the locally ordered B_2O_3 network, and the network configuration often adds non-bridging oxygens (NBOs). The distribution of the oxygen over the boron atoms no longer remains so uniform, and part of the boron atoms adopt modified co-ordination structure from BO_3 to BO_4 [10, 11]. A BO_4 group in the boroxol ring can be generated in several ways and it results in new diborate or triborate structural units, providing a modified spectrum of pure v-B_2O_3 of interconnected boroxol rings [9, 10, 18].

Thus, the bands A and B observed at 1480 and 1315 cm^{-1} in glass (c), in Fig. 1, using 3 mol% Ag_2O additive, and which compare very well in position with the Raman bands at 1475 and 1325 cm^{-1} of pure v-B_2O_3 [4], are unambiguously assigned to two different B–O stretching vibration modes in a boroxol ring, as we recently discussed in detail elsewhere [19]. In principle, the six-membered boroxol ring (with the effective molecular formula $B_3O_{4.5}$) exhibits six different B–O ring stretching vibrations, including the one-ring breathing-vibration mode, which is a totally symmetric and non-degenerate vibration, and therefore characteristically appears as a sharp and intense Raman band at ~808 cm^{-1} in pure and substituted borate glasses [1, 4, 8]. These vibrations (of which, of course, two are doubly degenerate) have characteristically strongly mixed characters and therefore were not resolved even in a crystalline B_2O_3. In the glasses, they are further modified (broadened by overlapping one over the other) in enhanced local interactions in irregular bridging of boroxol rings in the network in a random fashion. In this case, the lower frequency bands (here, bands C or D) are attributed to the B–O stretching vibrations involving (i) the oxygens

bridging two boroxol rings or bridging a ring to the network, and/or (ii) the oxygens in locally modified $BO_3 \rightarrow BO_4$ groups in the rings. The 1120 cm^{-1} band observed in the ternary glass, using no nucleation catalyst, thus represents the B–O stretching vibration in the $BO_3 \rightarrow BO_4$ modified group in the boroxol ring.

Whatever the assignments of the individual bands, an overall shift of the total absorption (i.e. $\sim 40\ cm^{-1}$ in the peak maximum and $\sim 120\ cm^{-1}$ in the onset of the zero absorption, Fig. 1) to higher frequencies, observed in the Ag_2O catalysed glasses, clearly demonstrates a reordering of the B_2O_3 network structure by considerably improved connectivity between the boroxol rings by effectively reduced numbers of $BO_3 \rightarrow BO_4$ modified groups and free NBOs. In this model, the increase in the magnitude of the B–O stretching frequencies, as observed here, is likely to be due to a decrease in the effective mass of the boroxol ring as the mass of the bridging oxygens is now shared with the adjoining units. When these units are decoupled into free boroxol rings, with one or more NBOs, the mass of the NBO(s) is confined to the associated boroxol ring, and that exhibits an increased effective mass. Hence, the NBO free boroxol rings always exhibit a lower effective mass (and higher B–O stretching frequencies) than the boroxol rings with one or more NBOs.

The band group observed at 800–600 cm^{-1} is assigned to the BOB angle bending vibration [1, 10]. It is shifted to lower values, i.e. in the opposite trend to the frequencies in the B–O stretching vibrations, from 740 cm^{-1} to 723 cm^{-1} and 718 cm^{-1} subsequent to adding 0.5 and 3 mol% Ag_2O, respectively, in the glass series. Of course, a change in position or mass of the bridging oxygens sensitively reflects in these two sets of frequencies with a linear relation

$$\gamma_{fn} = \gamma_n \left(\frac{\nu_n}{\nu_{fn}} \right)_{A,B} \quad (1)$$

where γ_{fn} and ν_{fn} are the frequencies in the bending and stretching vibrations, respectively, in the NBO-free boroxol ring (i.e. $n = 0$), and those γ_n and ν_n are for the boroxol ring with n NBOs, with the feasible values of $n = 1, 2$ or 3 in a pure boroxol ring of pure BO_3 groups. The ν_n and ν_{fn} measure almost the same ratio of $\nu_n/\nu_{fn} = 0.973$ in the B–O stretching bands A and B in two glasses a and c in Fig. 1. This ratio, with the observed value of $\gamma_n = 740\ cm^{-1}$ in glass a, in Equation 1, yields a value of the BOB angle bending frequency $\gamma_{fn} = 720\ cm^{-1}$ in glass c. The results provide an internal consistency of the present assignments that the B–O stretching bands A and B belong to the same structural units, i.e. the pure boroxol rings, and the band group at 718–740 cm^{-1} represents an average position of the corresponding bending vibrations. The improved bridging between the boroxol rings in a locally ordered network in the Ag_2O catalysed glasses does not resolve the overlapping structures of the bands, but it clearly caused, as expected, the bending vibration band to be sharper with a half-bandwidth $\sim 60\ cm^{-1}$ ($\sim 75\ cm^{-1}$ otherwise).

The network of the interconnected basis structural units in these substituted borate glasses provides an interconnected wetting layer to the reaction species (Ba^{2+} and Fe^{3+}) of $BaFe_{12}O_{19}$ so that they easily grow and precipitate in the stable $BaFe_{12}O_{19}$ crystals over the network. In the other case, these reaction species are irregularly trapped in between the small domains of the B_2O_3 network, unable to react together to yield the complete reaction at these temperatures. As expected, they rather locally crystallize in the separated domains and usually contain the by-product impurities of the recrystallized Fe_2O_3, barium borates, and other similar phases [6].

4.2. Infrared bands in $BaFe_{12}O_{19}$ microcrystals

The first doublet band-group of nearly equally intense components at ~ 595 and 560 cm^{-1} (in Figs 3 and 4) represents two resolved Fe^{3+}–O^{2-} stretching vibrations in the tetrahedral (FeO_4) sites while the second doublet band-group observed at $\sim 448\ cm^{-1}$ is due to the Fe^{3+}–O^{2-} stretching vibrations in the octahedral (FeO_6) sites of Fe^{3+} in the $BaFe_{12}O_{19}$ crystal lattice [11, 19]. Another band-group appeared at 350–360 cm^{-1}, which is considerably sharper than any of the above two band-groups, and it is assigned to one of the FeO_4 deformation vibrations according to the force field over the Fe^{3+}–O^{2-} bonds [19]. Other components of the FeO_4 or FeO_6 band-groups are at lower frequencies not studied here.

The $BaFe_{12}O_{19}$ belongs to a $P6_3/mmc$ hexagonal crystal structure [10, 20], with $Z = 2$ formula units per primitive unit cell, i.e. with a total of 24 Fe^{3+} cations, which occupy two different tetrahedral (including the pseudo-tetrahedral) and octahedral sites, i.e.

$$24\,Fe^{3+}\,(\text{total}) = 6\,Fe^{3+}\,(\text{tetra}) + 18\,Fe^{3+}\,(\text{octa}) \quad (2)$$

The ratio of Fe^{3+} cations in these two sites is Fe^{3+} (octa)/Fe^{3+} (tetra) = 3 [20, 21], but the infrared peaks in the two groups exhibit similar intensities for particles as large as 20 μm or larger (Fig. 4a and d), achieved by prolonged annealing at 795 °C, as summarized in Table I. This means that the FeO_4 tetrahedron has an enhanced infrared intensity value, particularly in the small-sized particles of micrometre order, caused by distortion in it by expected microscopic and macroscopic (electromagnetic) interactions between the crystallites and the glass matrix [22].

The distortion in the FeO_4 group in the $BaFe_{12}O_{19}$ crystal lattice is evident by removal of the T_d symmetry of the distortion-free FeO_4 group, which has four fundamental modes of vibration [19], one symmetric stretching ν_1 (A_1), one asymmetric stretching ν_3 (F_2), and two deformation modes ν_2(E) and ν_4(F_2). The vibration A_1 is non-degenerate while the vibrations E and F_2 are doubly and triply degenerate, respectively. All four vibration groups are allowed in the Raman spectrum but only ν_3 and ν_4 are allowed in the infrared. Obviously, the distortion has removed the degeneracy of the ν_3 mode, in this example, providing the two resolved bands of 560 and 595 cm^{-1} in it. It is this distortion-induced electric dipole moment, μ_e, which accounts for the intensities in these bands.

The Fe^{3+}–O^{2-} (FeO_4) bond oscillation eventually exhibits an ~ 1.7 times larger μ_e value per Fe^{3+} cation (as can be calculated from square root of the integrated intensities) over that in the FeO_6 group.

5. Conclusion

A small, $\leqslant 3$ mol%, Ag_2O additive in these glasses plays a crucial role in modifying local ordering of the boroxol rings by inhibiting $BO_3 \rightarrow BO_4$ group transformation with a reduced number of non-bridging oxygens in the structural units (boroxol rings) in the B_2O_3 network. These locally ordered glasses of regularly interconnected boroxol rings readily crystallize magnetic $BaFe_{12}O_{19}$ microcrystals, which have a higher coercivity $H_{ci} \sim 5000$ Oe (after finishing and thermal treatments of the final crystal sizes of ~ 1 μm), compared to the value for similar crystals prepared by other processes, with an usual value of the saturation magnetization $M_s = 71$ e.m.u. g^{-1}, at room temperature.

Acknowledgements

S. Ram gratefully acknowledges the fruitful discussion with Professor H. J. Fecht at T.U. Berlin and the financial support from the AvH Foundation, Germany.

References

1. F. L. GALEENER and M. F. THORPE, *Phys. Rev. B* **28** (1983) 5802.
2. E. I. KAMITSOS, *J. Phys. Chem.* **93** (1989) 1604.
3. R. A. BARRIO, F. L. C. ALVARADO and F. L. GALEENER, *Phys. Rev. B* **44** (1991) 7313.
4. A. K. HASSAN, L. M. TORELL, L. BÖRJESSON and H. W. DOWELDAR, *ibid.* **45** (1992) 12797.
5. Y. INAGAKI, H. MAEKAWA, T. YOKOKAWA and S. SHIMOKAWA, *ibid.* **47** (1993) 674.
6. S. RAM, D. CHAKRAVORTY and D. BAHADUR, *J. Magn. Magn. Mater.* **62** (1986) 221.
7. S. RAM, D. BAHADUR and D. CHAKRAVORTY, *ibid.* **67** (1987) 378.
8. M. IRION, M. COUZI, A. LEVASSEUR, J. M. REAU and J. C. BRETHOUS, *J. Non-Cryst. Solids* **31** (1980) 285.
9. J. KROGH-MOC, *Phys. Chem. Glasses* **6** (1965) 46.
10. S. RAM and K. RAM, *J. Mater. Sci.* **23** (1988) 4541.
11. *Idem*, *Infrared Phys.* **29** (1989) 895.
12. E. I. KAMITSOS, G. D. CHRYSSIKOS, A. P. PATSIS and M. A. KARAKASSIDES, *J. Non-Cryst. Solids* **131** (1991) 1092.
13. B. WANG, S. P. SZU and M. GREENBLATT, *ibid.* **134** (1991) 249.
14. K. HANEDA and A. H. MORRISH, *IEEE Trans. Magn.* **25** (1989) 2597.
15. S. RAM and J. C. JOUBERT, *ibid.* **28** (1992) 15.
16. C. H. L. GOODMAN, *Nature* **257** (1975) 370.
17. *Idem*, *Phys. Chem. Glasses* **26** (1985) 1.
18. W. SOPPE, F. ALDENKAMP and H. W. DEN HARTOG, *J. Non-Cryst. Solids* **91** (1987) 351.
19. S. RAM, *Phys. Rev. B* **51** (1995) 6280.
20. R. BARHAM, *Can. J. Chem.* **52** (1974) 3235.
21. S. RAM, *J. Magn. Magn. Mater.* **82** (1989) 129.
22. M. FUJII, M. WADA, S. HAYASHI and K. YAMAMOTO, *Phys. Rev. B* **46** (1992) 15930.

Received 7 June 1995
and accepted 12 August 1996